NOVEL VAMPIRE ALGORITHMS FOR QUANTITATIVE ANALYSIS OF THE RETINAL VASCULATURE

E. Trucco[1] *L. Ballerini*[1] *D. Relan*[2] *A. Giachetti*[3] *T. MacGillivray*[2] *K. Zutis*[1]
C. Lupascu[4] *D. Tegolo*[4] *E. Pellegrini*[1] *G. Robertson*[2] *P.J .Wilson*[5] *A. Doney*[6] *B. Dhillon*[7]

[1] CVIP, School of Computing, University of Dundee, UK
[2] CRIC, University of Edinburgh, UK
[3] Dipartimento di Informatica, University of Verona, Italy
[4] Dipartimento di Matematica e Informatica, University of Palermo, Italy
[5] Dept of Ophthalmology, Ninewells Hospital, Dundee, UK
[6] Biomedical Research Centre, Ninewells Hospital, Dundee, UK
[7] Princess Alexandra Eye Pavilion / University of Edinburgh, UK

ABSTRACT

This paper summarizes three recent, novel algorithms developed within VAMPIRE, namely optic disc and macula detection, artery-vein classification, and enhancement of binary vessel masks, and their performance assessment. VAMPIRE is an international collaboration growing a suite of software tools to allow efficient quantification of morphological properties of the retinal vasculature in large collections of fundus camera images. VAMPIRE measurements are currently mostly used in biomarker research, i.e., investigating associations between the morphology of the retinal vasculature and a number of clinical and cognitive conditions.

1. INTRODUCTION

We present three novel algorithms for optic disc (henceforth OD) and macula detection, artery-vein (A-V) classification, and enhancement of binary vessel masks, developed within the VAMPIRE retinal image analysis project, an international collaboration of 10 clinical and image processing centres [1]. The VAMPIRE software suite aims to allow efficient quantification of morphological features of the retinal vasculature in large sets of fundus camera images, generating measurements used for biomarker discovery. Biomarkers are measurements that associate, in a statistical sense, with measurements related to specific conditions [2, 3, 4]. Examples using VAMPIRE software include [5] (lacunar stroke) and [6] (cognitive ageing), and ongoing VAMPIRE studies impact sarcopenia, schistosomiasis and gene expression.

A fundamental requirement of biomarker research is access to large data quantities to achieve sufficient power and significance. Measuring typical retinal quantities like vessel width, tortuosity and branching angles manually is extremely time-consuming; some quantities like the fractal dimension cannot even be measured by hand. This is the basic motivation for semi-automatic software tools generating reliable measurements efficiently.

For our purposes here, we can identify two parts in the growing literature of computer-assisted retinal image analysis (henceforth RIA; see [7] for a recent, exhaustive survey), one devoted to assisting diagnosis, the other to biomarker discovery. Both require the location of retinal landmarks to set up retinal co-ordinates, as well as specialized measuring algorithms. We present three novel such algorithms.

(1) OD and macula location. We propose a novel algorithm based on inpainting and a symmetry transform, which performs very competitively in tests with a public data set and images from our local diabetes screening program.
(2) A-V classification. We show that an expectation-maximization algorithm with Gaussian mixture models, using a few discriminative features, achieves good performance.
(3) Vessel mask enhancement. Vessel contours in binary masks generated by vessel location algorithms are typically irregular. We introduce a novel algorithm, with closed-form solution, performing splined-based smoothing of local contours under a parallelism constraint.

Given space limits, we only summarize validation results for each algorithm. We notice that the RIA validation is a topic of fundamental importance and still under discussion in the community: no universally accepted protocol exists to declare performance satisfactory (itself a debated concept) of RIA algorithms. The reader is directed to the recent international discussion and proposal reported in [8].

2. OPTIC DISC AND FOVEA DETECTION

The new detectors for OD and fovea exploit bright-dark circularly symmetric structures in vessel-removed, inpainted monochrome images. The symmetry cue proves more resilient to varying mage quality than classical template-based localization, and does not rely heavily on contextual cues possibly absent in low-quality images. The method exploits the fact that the OD is crossed by large vessels, and the fovea located in an avascular zone.

The input image is converted to grayscale. Vessels are removed using the inpainting procedure described in [9]. Dark or bright radial symmetries are captured by the Fast Radial Symmetry transform by Loy and Zelinsky [10]. For each radius R in a defined range and for each pixel location $\vec{p}$, a *positively affected* pixel p_+ and a *negative affected* pixel p_- are obtained translating $\vec{p}$ along the gradient direction in positive (dark to bright) and negative (bright to dark) orientations. Values of the bright (OD) and dark (fovea) symmetry maps are generated by accumulating in "affected" pixels values depending on the gradient magnitude of the originating points and filtering maps in order to make the contribution scale invariant, and summing the contributions of all the radii used. If radii are densely

sampled, the transform captures well all the symmetric structures in the range used. For OD detection we compute the "positive" symmetry map S^+ on all integer radius values within 7 and 12 pixels in a subsampled image where the expected OD radius is approximately 10 pixels (Fig. 1 D). For the macular region, also usually symmetric in its inner structure, we compute the "negative" symmetry map S^- in the range 3-12 pixels (Fig. 1 E).

To avoid false detections due to bright circular spots, pathologies or dark vessels, we multiply the symmetry map by a vessel-dependent weight function. Here the likelihood for a pixel to be the OD centre is given by:

$$p_{OD}(x,y) = S^+(x,y) \cdot max(0.1, V(x,y)) \quad (1)$$

where $V(x,y)$ is the vessel density function obtained by convolving a vessel segmentation mask (Fig. 1 B) with a circular kernel, saturated to 1 when the vessel density is above a threshold (Fig. 1 C).

Similarly, the fovea detector estimates the likelihood for an image point to be the fovea centre as:

$$p_F(x,y) = S^-(x,y) \cdot (1 - V(x,y)) \quad (2)$$

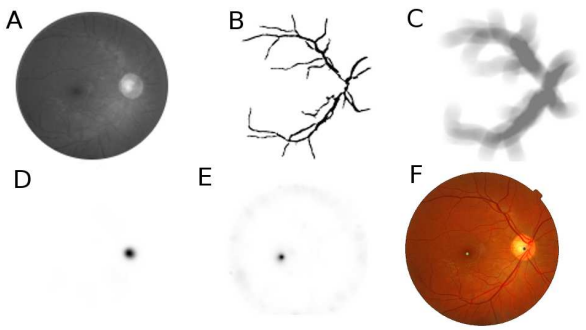

Fig. 1. OD and fovea localization steps: A: Grayscale inpainted image. B: Major vessels segmentation. C: Vessel density. D: Positive Fast Radial Symmetry Map computed with rays in a range including the expected OD size (7-12 pixels of the subsampled image). It presents a sharp maximum near the true OD centre. E: Negative part of the Fast Radial Symmetry computed with rays in a wide range 3-12 pixels. F: detected OD and fovea centres superimposed to the original image.

We tested the algorithm with 300 MESSIDOR images (http://messidor.crihan.fr) that we had annotated by three ophthalmologists using VAMPIRE annotation tools. We compared the locations of manual and automatic OD centres. Following the recent literature, we considered the OD detected correctly if the distance between automatic and manual centres was less than half of the expected average OD diameter, i.e., 200 pixels at the original resolution [11]. The detection rate was 100% despite the presence of images with poor quality and artefacts.

Fovea centre detection was validated on 117 images acquired from the Tayside diabetic screening program. Images were 3504×2336 pixels and type-2 field (macula-centred). The images were divided into three quality classes, good (67), medium (30), and difficult (20), by a trained observer who also annotated the fovea centre. Quality was determined by the visibility and integrity of the macular region. To compare results with previous work we considered the fovea detected successfully if the distance between manual and automatic centres was lower than 1/4 of the OD diameter. The percentage of correct detections was 97.4%, (100% for the good subset, 96.7% for the medium and 95% for the difficult one, considerably higher than the 68.6% obtained with the technique previously implemented within the VAMPIRE framework [12].

	OD center (300 images)	fovea center (107 images)
avg error (%OD radius)	12.6	32.6
std. dev.	9.0	31.8
median error	10.5	23.8
detection rate (%)	100	97.5

Table 1. Average errors (distance between estimated and annotated points/expected OD size), standard deviations, median errors and detection rates for OD and fovea centres on the two annotated datasets.

The results obtained compare favourably with the literature; e.g., in similar conditions, Niemejier et al. [13] reported detection rates between 93% and 99.4% for OD and 89% and 96.8% for the fovea. We notice that no images have been removed from the image groups annotated by our experts, including cases with pathologies. The new OD and fovea detectors are currently being validated on larger datasets. The symmetry-based OD detector is now the default method to initialize the accurate OD segmentation technique ([9]).

3. ARTERY-VEIN CLASSIFICATION

We concentrate on the major veins and arteries in Zone B, the region surrounding the OD normally used in retinal biomarkers studies (Figure 2(a)) [5, 14, 15]. We deploy a Gaussian mixture model, an expectation-maximization unsupervised classifier, and a quadrant-pairwise approach.

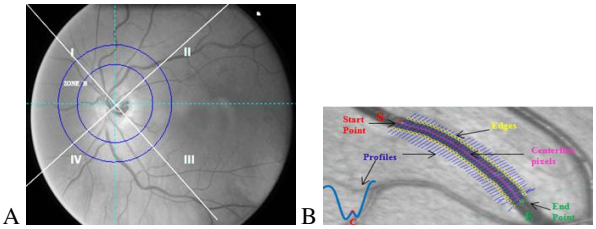

Fig. 2. (a) Quadrants and Zone B (annulus around OD). (b) Illustration of main elements in boundary refinement.

To counteract inter- and intra-image contrast, luminosity and colour variability, we first compensate for background illumination in the red, green and hue channels [16]. The illumination-corrected images are then processed to extract colour intensity features from vessel centreline pixels. In addition, the hue channel is processed before illumination correction in order to improve vessel contrast. To extract centreline pixels, a start and an end point (S and E resp.) are selected manually and the intervening vessel is tracked (Figure 2(b)).

To achieve this, we locate a point P_{new}, 5 pixels ahead of S towards E (i.e., with direction from S to E), and obtain the intensity profile across the vessel axis at P_{new} (Figure 2(b)). The approximate midpoint of the vessel, C (marked red on the intensity profile) is then found. The procedure is iterated with a new direction (from C to E), V_{C-E}, and so on until the end point E is reached. Thus we obtain cross-sectional intensity profiles at every 5th pixel between S and E

(blue lines in Figure 2(b)). A Canny edge detector is then applied to each profile to locate vessel edges (yellow in Figure 2(b)). The final centerline pixels (pink in Figure 2(b)) are located as the midpoints of each pair of edge points.

The image was divided into four quadrants by locating the OD and its approximate diameter [9]. After locating vessel centrelines in each quadrant, four colour features are computed from the illumination-corrected image in a circular neighbourhood around each vessels centreline pixels, with diameter 60% of the mean vessel diameter. The features are the most significant ones reported in various studies [2, 3, 4]: the mean of red (MR), mean of green (MG), mean of hue (MH) and variance of red (VR). After feature extraction, there are four sets of feature vectors $F_q, q = 1, \ldots, 4$, for each pair of quadrant (I, II), (II, III), (III, IV) and (IV, I). Working on pairs of quadrants is a compromise between localizing features (avoiding variations due to location and not to vessel class) and guaranteeing the presence of at least one artery and one vein. Finally, each set F_q of colour features is classified using an EM classifier with a Gaussian Mixture Model (GMM-EM). As stated above, the classification is performed separately on pairs of quadrant. We tested our classifier with 406 vessels from 35 colour fundus images. The system did not assign a final label (artery or vein) to 55 vessels, i.e. 13.5% were classified not labeled. 92% of the remaining 351 vessels (which were assigned a label of artery or vein) were classified correctly.

To assess performance, we compared the automatic results with manual labels from two clinicians at two different experience levels (student and consultant), for which no adjustment was applied. We estimated performance parameters following [4], resulting in sensitivity 0.8182-0.7688, specificity 0.8978-0.9591), and accuracy 0.8719-0.8547, where the two figures refer to results for arteries and veins respectively (e.g., arteries specificity - veins specificity).

4. ENHANCEMENT OF BINARY VESSEL MASKS

We introduce a costrained spline-fitting algorithm to refine vessel contours in raw binary maps obtained from vessel detectors, and show a large improvement of vessel width estimation with the main public data set for this task, REVIEW [17].

First, a temporary skeleton is obtained using morphological thinning on the binary mask; branching points are removed and a natural cubic spline is fitted to the thinned centreline. Second, two coupled cubic splines are fitted to the original (jagged) contours by solving a linear system overconstrained by a parallel-tangent constraint coupling the two splines and penalizing locally non-parallel contours. The system can be written as:

$$\begin{cases} y_A = a_i(x - x_{A,i})^3 + b_i(x - x_{A,i})^2 + c_i(x - x_{A,i}) + d_i \\ y_B = \alpha_i(x - x_{B,i})^3 + \beta_i(x - x_{B,i})^2 + \gamma_i(x - x_{B,i}) + \delta_i \\ y'_A(x_{A,i+1}) = y'_B(x_{B,i+1}) \end{cases} \tag{3}$$

where the spline knots $(x_{A,i}, y_{A,i})$ and $(x_{B,i}, y_{B,i})$ are n pairs of coupled contour points, and the last equation is the parallelism constraint.

Finally, the vessel width w_j at point C_j lying on the spline-smoothed centreline is estimated computing the Euclidean distance between points D_j and E_j on the two refined contours and lying on segment d_j, orthogonal to the centreline at C_j [18].

We tested our constrained spline fit by applying it to width estimation from binary vessel masks. We used the public REVIEW database [17], whose four image sets offer a representative spectrum of vessel appearance in fundus images: high-resolution (HRIS dataset), central light reflex (CLRIS dataset), vascular diseases (VDIS dataset) and kickpoints (KPIS dataset). Three experts (observers O_1, O_2 and O_3) marked manually vessel edge points and the average of the three width estimates is considered as the ground truth width. REVIEW contains 5066 profiles. For comparison of different algorithms, the error χ_i is defined as $\chi_i = w_i - \psi_i$ where w_i is the width at ith location estimated by the algorithm under examination. The standard deviation σ_χ of the error is used to evaluate algorithm performance and considered more important than the mean [19]. A further useful parameter for performance evaluation is the success rate (SR), i.e. the number of meaningful measurements returned by the algorithm over the total number of profile reported in the database.

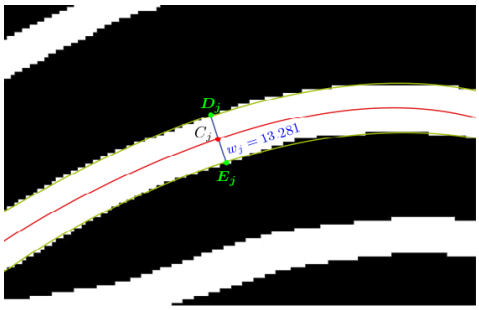

Fig. 3. Vessel width at C_j estimated as the Euclidean distance w_j between D_j and E_j.

Table 2 reports the performance of our method and its comparison with recent algorithms: Extraction of Segment Profiles (ESP) procedure [19] and Xu's graph-based method [20]. The performance achieved by our simple double-spline fit with parallelism constraint at knots is comparable and sometime better to that of specialized, sophisticated width estimation algorithm.

5. CONCLUSIONS

We have presented briefly three algorithms recently developed within the VAMPIRE project, for OD/fovea detection, A-V classification and enhancement of binary vessel masks. Two have been incorporated in the VAMPIRE software suite and are used in current clinical studies on retinal biomarkers. The OD/fovea detection introduces a novel combination of symmetry detection and inpainting, leading to competitive results compared with the recent literature. Our A-V classifier show that an expectation-maximization algorithm with Gaussian mixture models achieves good performance using only a few discriminative features. Our novel contour-smoothing technique, based on spline fitting with a parallelism constraint,improves dramatically the accuracy of width estimation taken directly from unprocessed binary masks from a standard vessel detector, in tests with the standard public data set, REVIEW. Current VAMPIRE work includes validation of these modules with larger, annotated data sets.

Acknowledgements

This work is partially supported by Leverhulme Trust grant RPG-419 "Discovery of retinal biomarkers for genetics with large cross-linked datasets".

Table 2. Performance comparison of the width measurement methods on the REVIEW database

Method	Measurement		Error		SR %	Measurement		Error		SR %
	μ	σ	μ_χ	σ_χ		μ	σ	μ_χ	σ_χ	
	HRIS					CLRIS				
First observer: O_1	4.12	1.25	-0.23	0.288	100	13.19	4.01	-0.61	0.567	100
Second observer: O_2	4.35	1.35	0.002	0.256	100	13.69	4.22	-0.11	0.698	100
Third observer: O_3	4.58	1.26	0.23	0.285	100	14.52	4.26	0.72	0.566	100
Ground truth: O	4.35	1.26	-	-	100	13.80	4.12	-	-	100
ESP [19]	4.63	-	0.28	0.420	99.7	15.7	-	-1.90	1.469	93.0
Graph [20]	4.56	1.30	0.21	0.567	100	14.05	4.47	0.08	1.78	94.1
Proposed method	**3.93**	**1.40**	**-0.42**	**0.760**	**95.7**	**13.81**	**3.68**	**-0.16**	**1.229**	**90.2**
	VDIS					KPIS				
First observer: O_1	8.50	2.54	-0.35	0.543	100	7.97	0.47	0.45	0.233	100
Second observer: O_2	8.91	2.69	0.06	0.621	100	7.60	0.42	0.08	0.213	100
Third observer: O_3	9.15	2.67	0.30	0.669	100	7.00	0.52	-0.53	0.234	100
Ground truth: O	8.85	2.57	-	-	100	7.52	0.42	-	-	100
ESP [19]	8.80	-	-0.05	0.766	99.6	6.56	-	-0.96	0.328	100
Graph [20]	8.35	3.00	-0.53	1.43	96.0	6.38	0.59	-1.14	0.67	99.4
Proposed method	**8.17**	**2.82**	**-0.79**	**1.381**	**92.1**	**6.06**	**0.28**	**-1.32**	**0.319**	**93.9**

References

[1] A Perez-Rovira, T MacGillivray, E Trucco, K S Chin, K Zutis, C Lupascu, D Tegolo, A Giachetti, P J Wilson, and A Doney, "Vampire: Vessel assessment and measurement platform for images of the retina," in *proc. IEEE Engineering in Medicine and Biology Society*. 2011, pp. 3391–3394, IEEE.

[2] E. Grisan and A. Ruggeri, "A divide et impera strategy for automatic classification of retinal vessels into arteries and veins," in *Proc. 25th IEEE Intern Conf on Engineering in Medicine and Biology*, 2003, pp. 890–893.

[3] H. F. Jelinek, C. Depardieu, C. Lucas, D. J. Cornforth, W. Huang, and M. J. Cree, "Towards vessel characterisation in the vicinity of the optic disc in digital retinal images," in *Proc. New Zealand Image and Vision Computing Conf.*, 2005.

[4] M. Saez, S. Gonzlez-Vzquez, M Gonzalez-Penedo, M A Barcelo, M Pena-Seijo, G Coll de Tuero, and A Pose-Reino, "Development of an automated system to classify retinal vessels into arteries and veins," 2012.

[5] F. N. Doubal, T. J. MacGillivray, P. E. Hokke, B. Dhillon, M. S. Dennis, and J. M. Wardlaw, "Differences in retinal vessels support a distinct vasculopathy causing lacunar stroke," *Neurology*, vol. 72, pp. 1773–1778, 2009.

[6] N. Patton, T. Aslam, T. J. MacGillivray, A. Pattie, I. J. Deary, and B. Dhillon, "Retinal vascular image analysis as a potential screening tool for cerebrovascular disease," *Journal of Anatomy*, vol. 206, pp. 318–348, 2005.

[7] M. Abramoff, M Garvin, and M Sonka, "Retinal imaging and image analysis," *IEEE Reviews in Biomedical Eng.*, vol. 3, pp. 169–208, 2010.

[8] E. Trucco et al. (19 authors), "Validation of automatic retinal image algorithms: issues and a proposal," *Investigative Ophthalmology and Visual Science*, vol. to appear, 2013.

[9] A Giachetti, KS. Chin, E Trucco, C Cobb, and PJ. Wilson, "Multiresolution localization and segmentation of the optical disc in fundus images using inpainted background and vessel information," in *ICIP*, 2011, pp. 2145–2148.

[10] G Loy and A Zelinsky, "Fast radial symmetry for detecting points of interest," *IEEE Trans. Pattern Anal. Mach. Intell.*, vol. 25, pp. 959–973, August 2003.

[11] H. Yu, S. Barriga, C. Agurto, S. Echegaray, M. Pattichis, G. Zamora, W. Bauman, and P. Soliz, "Fast localization of optic disc and fovea in retinal images for eye disease screening," in *Proc. SPIE 7963, Medical Imaging 2011*, 2011, pp. 796317–796317–12.

[12] K S Chin and E Trucco, "Fovea detection using anatomical priors and vessel density," in *Proc. Ophthalmic Workshop, Univ of Liverpool*, 2011.

[13] M Niemeijer, MD Abrmoff, and B van Ginneken, "Fast detection of the optic disc and fovea in color fundus photographs," *Medical Image Analysis*, vol. 13, no. 6, pp. 859 – 870, 2009, Special Section on Computational Biomechanics for Medicine.

[14] Wong T. Y, Knudtson M. D., Klein R., Klein B. E. K., Meuer S. M., and Hubbard L. D, "Computer-assisted measurement of retinal vessel diameters in the Beaver Dam eye study: methodology, correlation between eyes, and effect of refractive errors," *Ophthalmology*, vol. 111, no. 6.

[15] H. Leung, "Relationships between age, blood pressure, and retinal vessel diameters in an older population," *Invest. Ophthalm. and Visual Science*, vol. 44, no. 7, pp. 2900–4, 2003.

[16] M. Foracchia, E. Grisan, and A. Ruggeri, "Luminosity and contrast normalization in retinal images," *Medical Image Analysis*, vol. 9, no. 3, pp. 17990, 2005.

[17] B. Al-Diri, A. Hunter, D. Steel, M. Habib, T. Hudaib, and S. Berry, "REVIEW-A reference data set for retinal vessel profiles," 2008, pp. 2262–2265.

[18] A. Cavinato, *Spline-based refinement of contours in binary maps of retinal vessels*, Tesi di laurea triennale, University of Padova, Sept. 2012.

[19] B. Al-Diri, A. Hunter, and D. Steel, "An active contour model for segmenting and measuring retinal vessels," vol. 28, pp. 1488–1497, Sept. 2009.

[20] X. Xu, M. Niemeijer, Q. Song, M. Sonka, M. K. Garvin, J. M. Reinhardt, and M. D. Abramoff, "Vessel boundary delineation on fundus images using graph-based approach," vol. 30, no. 6, pp. 1184–1191, 2011.